Deep Mining 2024 – P Andrieux & D Cumming-Potvin (eds)

doi:10.36487/ACG_repo/2465_12

Assessing three different mining periods through the energy release rate at the Lucky Friday mine

Mathieu Armatys [a,*]

[a] *Corporate Technical Services, Hecla Mining Company, USA*

Abstract

The Lucky Friday mine (Idaho, USA) uses narrow underhand mining methods to extract stacked sub-vertical, tabular (silver, lead, zinc) ore veins from the Gold Hunter (GH) deposit within the St-Regis/Wallace Formations. The GH deposit has been in production since 1997 and has sustained full production for the mine since 2003 after withdrawing from the historical Lucky Friday deposit. The GH lies 1.5 km northwest of the latter. As of 2021, the current mining depth positions the leading mining front of the GH at 2.3 km relative to the surface. The mine front deepens by ~25 vertical metres per year at ~1,000 ore tonnes per day. Over two decades of mining have carved the current mined-out geometry, which includes several remnant pillars. When investigating the seismic output from production trends, three distinct periods arise. The first mining period (1997–2016) includes extraction done by the traditional underhand cut-and-fill mining method. The second mining period (2017–2019) presents a unique case where production was essentially reduced to incremental mining due to a work stoppage. The third mining period (2020–2021) accounts for extraction performed by the new underhand closed bench (UCB) method. Using a calibrated boundary element model, the yearly energy release rate (ERR) was calculated for each mining period and compared to the seismic energy release recorded by the mine-operated seismic system. As expected, the maximum seismic efficiency (defined as the quotient of recorded seismic energy by simulated elastic kinetic energy) per period is under 0.2%, which compares with results found in the literature. However, the three mining periods showed significant variations to infer a change in rock mass response due to the mining method. Finally, an attempt was made to fit the Lucky Friday results into the COMRO's empirical ERR graph, showing the relationship between the frequency of seismic events per area mined and the energy release rate in longwall mining of gold reefs in South Africa.

Keywords: *boundary element method, deep-mining, energy release rate, mine-induced seismicity*

1 Introduction

The Lucky Friday mine is located in Mullan, Idaho (USA), which initiated high-grade silver, lead and zinc production in 1942 and has been fully operated by Hecla since 1958. The mine hosts two distinct ore bodies, namely the Lucky Friday (LF) and the Gold Hunter (GH) deposits. The (founding) LF deposit rests in the Revett Formation, while the GH deposit sits in the Wallace Formation. Both formations emerged during the Middle Proterozoic (ca. 1.45–1.40 Ga) of the late Precambrian. The district's rocks are primarily belt series quartzites, where shallow water sediments metamorphosed into quartzites, siltites, and argillites. The Revett Formation (LF deposit) encompasses most of the stronger quarzitic rock, vertically-bedded (vitreous) quartzite that grades to an argillic-quartzite, characterised by a brittle-type failure response. The Wallace Formation (GH deposit) consists of softer rock (with less quartzite), vertically-oriented, thinly-bedded argillites, and argillite alternating with silt caps and local siltites, exhibiting a ductile response.

The present-day LF operations mine solely the GH deposit, which initiated cut-and-fill production in 1997 and relieved production from the (historical) LF deposit in 2003. The GH resides ~1.5 km northwest of the LF deposit

* Corresponding author. Email address: marmatys@hecla.com

and contains sub-vertical, stacked mineralised veins. Production occurs on the (main) 30-Vein and the (secondary) Intermediate-Veins. The 30-Vein has the most prolific grade within the mineralised packet of the GH. The main vein strikes ~110° for 670 lateral metres and dips ~85° (to the south), extending over 640 vertically mined metres with measured resources extending several hundred metres deeper. The continuous 30-Vein is narrow, mined at about 3 m thick, but can widen up to 6 m locally on several stope accesses. The Intermediate-Veins are similar in characteristics but less continuous on lateral and vertical extents. They are offset to the north of the 30-Vein and account for less than 25% of the total daily production. At ~1,000 tonnes per day (tpd), the GH's mining fronts deepen by ~25 vertical metres (total) annually.

Figure 1 shows the longitudinal view of the GH for the 2021 year-end geometry. Overall, the excavated geometry remains simple except for remnant pillars, which disrupt its continuity. Three distinct mining periods have occurred during the two decades of mining the 30-Vein. During the first mining period (1997–2016), extraction was carried out using the traditional underhand/overhand cut-and-fill mining method, referred to as the Lucky Friday Underhand Longwall (LFUL). The first period produced, on average, 720 tpd from the 30-Vein. The second mining period (2017–2019) was characterised by a significant reduction in production to 110 tpd due to a work stoppage, resulting in incremental mining. The third mining period (2020–2021) involved extraction using the newly developed underhand closed bench (UCB) mining method (Hecla 2023), restoring production on the 30-Vein to 630 tpd for the third period.

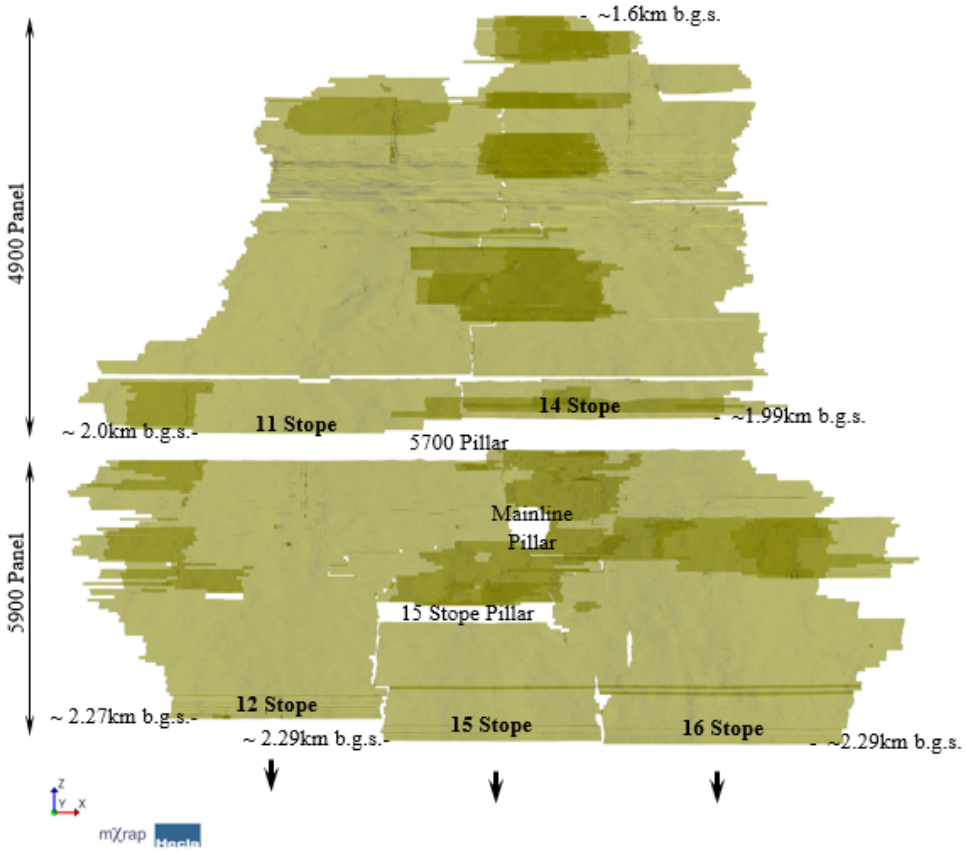

Figure 1 Longitudinal view of Gold Hunter 30-Vein and Intermediate-Veins (shaded), looking north. Capture of the as-built geometry for 2021 year-end. Inset arrows indicate the direction of mining

From the literature, the rock mass response to mining a deep-continuous, narrow tabular deposit consists of sustained closure observed in previously excavated stope boundaries (Malan 1999) and high-stress concentrations at the mining face (Budavari 1983). Field measurements at the mine have recorded up to 7.5 cm (~2.5% stain) of wall-to-wall closure in a top cut after extracting a lower underhand cut past the instrumented area (Raffaldi et al. 2019). On the other hand, visible rock yielding via tensile fracturing in stope headings confirms a high-stress environment living in the 30-Vein abutment (i.e. the mining front).

In addition, as captured by the mine-operated seismic system, large seismicity emerged in 2007, about 10 years after initiating extraction in the GH.

Therefore, this analysis rests on the opportunity to link three distinct mining periods with past production and seismic records.

2 Methodology

This section covers the analytical and numerical procedures for generating a mine-wide grid-based model, allowing to compare modelled results with seismic records for the three distinct mining periods.

2.1 Energy release

The energy release rate (ERR) was empirically derived to estimate seismic hazards of mining layouts in deep, seismically active, reef-type mines in South Africa (Cook et al. 1966). The analytical solution for ERR associates the total stress residing inside a block of ground to be mined and the induced boundary closure after removing the block with a seismic release potential. The mechanical work is obtained by multiplying half the pre-mining normal stress with the post-mining-induced closure, expressed as energy over the area mined (MJ/m^2). The ERR provides a practical (deterministic) way to forecast the seismic potential for specific extraction sequences or layouts in tabular mines.

The ERR directly relates to the energy released (W_r) of Salamon's energy balance components (Salamon 1984). If the work done on the support is ignored, the W_r component accounts for the surplus energy the rock mass dissipates after mining has proceeded, expressed as strain energy (MJ).

Expanded further, the W_r accounts for two independent energy-consuming parameters:

1. The violent kinetic energy release (W_k).
2. The non-violent strain energy loading (U_m).

The W_k component relates to the seismic energy (E_s) recorded by the seismic acquisition system (Hedley 1992). The U_m component reflects the energy stored in the mined block.

The ERR is applied in practice at other tabular mines (Scheepers et al. 2012; Hofmann 2012; Scheepers 2022).

2.2 Boundary element model setup

Map3D-v68 (Wiles 2022) serves as the grid-based boundary element model (BEM) code for the energy release analyses. Map3D doesn't assume any edge correction processes; however, further verifications determined a computational error of only ~2.5% between the theoretical and numerical ERR values (Armatys 2023). The Displacement Discontinuity (DD) elements were assumed for the stope mesh construct, where each element has a dimension of 3.05 × 3.05m with a virtual thickness of 3.05 m. The mesh resolution matches typical cut-and-fill stope advances. The capital infrastructures (ramps, main haulages, slot accesses) were ignored in the construction.

The complete mining geometry of the 30-Vein was reconstructed for the 1997 to 2021 year-end mining period (Figure 2). Mining progressed on the 11, 12, 14, 15, 16 Stopes on the 30-Vein, and 8 Stope on the 80-Vein (included due to its proximity with the remnant 5,700 Pillar). The extraction sequence was set to match production records obtained from field surveys and production tonnages. The final mining step assumed yearly increments, producing 26 distinct modelling steps which were regrouped into their associated mining periods.

As the model runs through each mining step, all the newly extracted DD elements get tagged to their respective extraction step with their numerical values. The model outputs the pre-mining normal stress and the post-mining-induced closure at each DD element's centre. The ERR is, upon extraction, calculated across the individual DD element assuming the following formulation:

$$ERR_{i,j} = \frac{1}{2} \times \sigma_{n_{i,j-1}} \times \delta_{n_{i,j}} \quad (1)$$

where:

ERR = energy release rate acting on the DD element [MJ/m^2].

σ_n = stress normal to the DD element [MPa].

δ_n = displacement normal to the DD element [m].

i,j = block number of DD element block, and mining step number, respectively.

The ERR is further decomposed into the kinetic energy release component through the following formulations, derived from Salamon (1983, 1984) and Hedley (1992), and adapted to the BEM:

$$W_{r_{i,j}} = ERR_{i,j} \times \Delta A_i \quad (2)$$

$$U_{m_{i,j-1}} = \sigma_{n_{i,j-1}}^2 \times \frac{(1-v^2)}{2E} \times \Delta A_i \times \Delta w_i \quad (3)$$

$$W_{k_{i,j}} = W_{r_{i,j}} - U_{m_{i,j-1}} \quad (4)$$

where:

W_r = strain energy released by extraction on the DD element [MJ].

ΔA = area assigned to the DD element [m^2].

U_m = strain energy computed on the pre-mined DD element [MJ].

Δw = mining width (thickness) of the DD element [m].

Based on these equations, the ERR and W_k components were post-processed outside the numerical model code. They were further averaged over yearly time steps and grouped into their associative mining periods. A data visualiser (GEM4D [Basson 2021]) was used to visually compare the output results with seismic records.

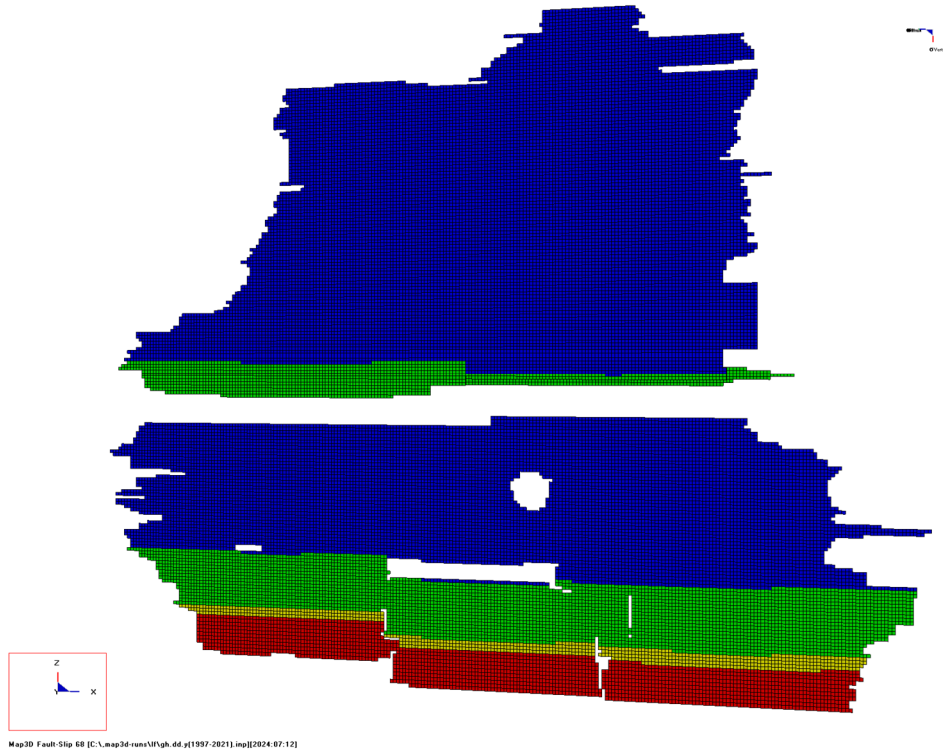

Figure 2 Longitudinal view of the grid-based model (DD element), looking north. Reconstruction of the main 30-Vein of the Gold Hunter deposit for the 1997-2011 (blue), 2013-2016 (green), 2017-2019 (yellow) and 2020-2021 (red) mining periods

3 Data

This section provides the available data gathered while mining the GH and defines the input parameters for the numerical modelling.

3.1 Seismic catalogue (1997–2021)

Seismic data was obtained from mine records. Pre-2013, the MP250 helicorder (from Electro-Lab) was used at the mine to estimate event location and local magnitude (ML). In 2013, the mine upgraded to an entire waveform digitising system (from ESG), which records the complete set of source parameters, such as seismic energy (E_S) and magnitudes (MW), and provides more accurate event locations with a source location error of less than 12 m. Only large events (≥ +1 Magnitude) were investigated per mining period. Therefore, no zoning attempts were undertaken, and all large events were assumed to be associated with mining during the period. Since both magnitude types are similar above this scalar threshold, this study assumes that MW and ML are equivalent, with figures reporting magnitudes in equivalent MW.

3.2 BEM input properties

The rock mass is assumed to be homogeneous, excludes discrete discontinuities and is set in an infinitely elastic medium where E and υ are the primary input parameters. The Young's modulus controls the amount of closure measured in-stope. Therefore, a numerical calibration effort was undertaken to determine the best fit between numerical and in-field closure records taken in 11 and 15 Stope (Raffaldi et al. 2019). Figure 3 shows the most favourable match on closure at E = 29.4 GPa with an overall root mean square error (RMSE) of 2.16 cm (Armatys 2023). This modulus of elasticity was used throughout this study. The Poisson ratio was set to 0.2.

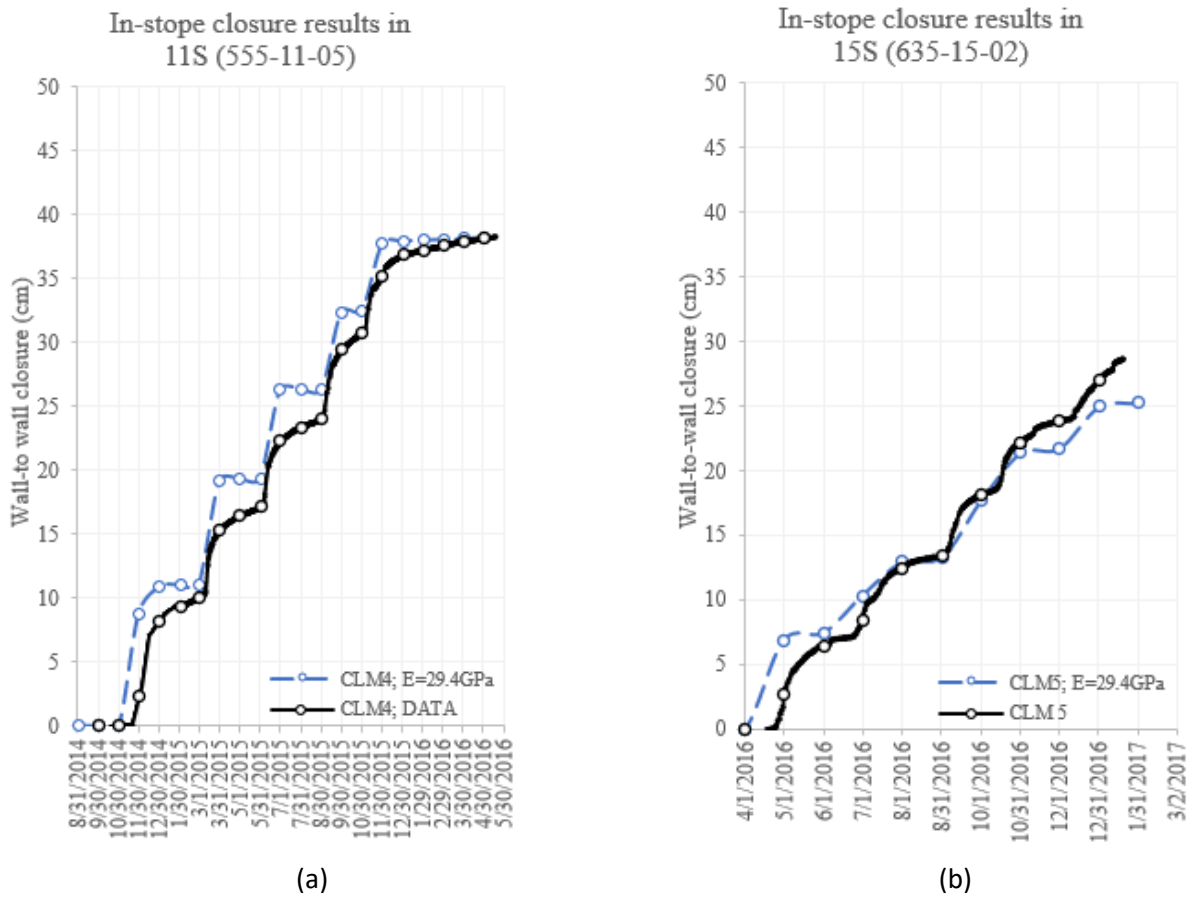

Figure 3 Comparison between in-field stope measurements (black trace) and simulated (blue trace) best-fit normal displacement at E = 29.4 GPa. (a) in 11 Stope; (b) in 15 Stope

The BEM construct assumes the following in situ stresses (in MPa):

$$\sigma_3 = 0.029 \times z + 8.8 \quad (5)$$

$$\sigma_2 = 1.200 \times \sigma_3 \quad (6)$$

$$\sigma_1 = 1.500 \times \sigma_3 \quad (7)$$

With σ_3 set vertically, σ_2 oriented N50°E and σ_1 oriented N40°W. Note that z refers to depth (in metres) below ground surface while the constant (8.8) accounts for the extra 305 m of overburden above the GH deposit.

4 Results

This section presents the ERR and Wk outputs and links them to large seismic events and tonnages recorded during mining the 30-Vein.

4.1 Energy release per mining period

Figure 4 shows the computed ERR and W_k per (extracted) DD element for the 2016 mining sequence as an example of the output data. As a reference, the large seismic events that occurred during that period were all projected onto the 30-Vein. In this case, the 2016 extraction assumed monthly increments (i.e. the model ran in 12 mining-steps for that period). As can be seen, the individual energy releases vary throughout the mined-out geometry; the ERR ranges between 9–90 MJ/M^2, while the W_k falls between 40–360 MJ. Locally, the higher energy outputs crudely match the location of large, recorded seismic occurrences. However, each stope presents its specific seismic threshold or onset. It is also worth noting that upper remnant pillars continue to release seismicity, with little to no mining in proximity (> 100 m). These distal events are likely attributed to cumulative incremental stress changes occurring in these remnant geometries, triggered by mining the lower abutments over a significant period

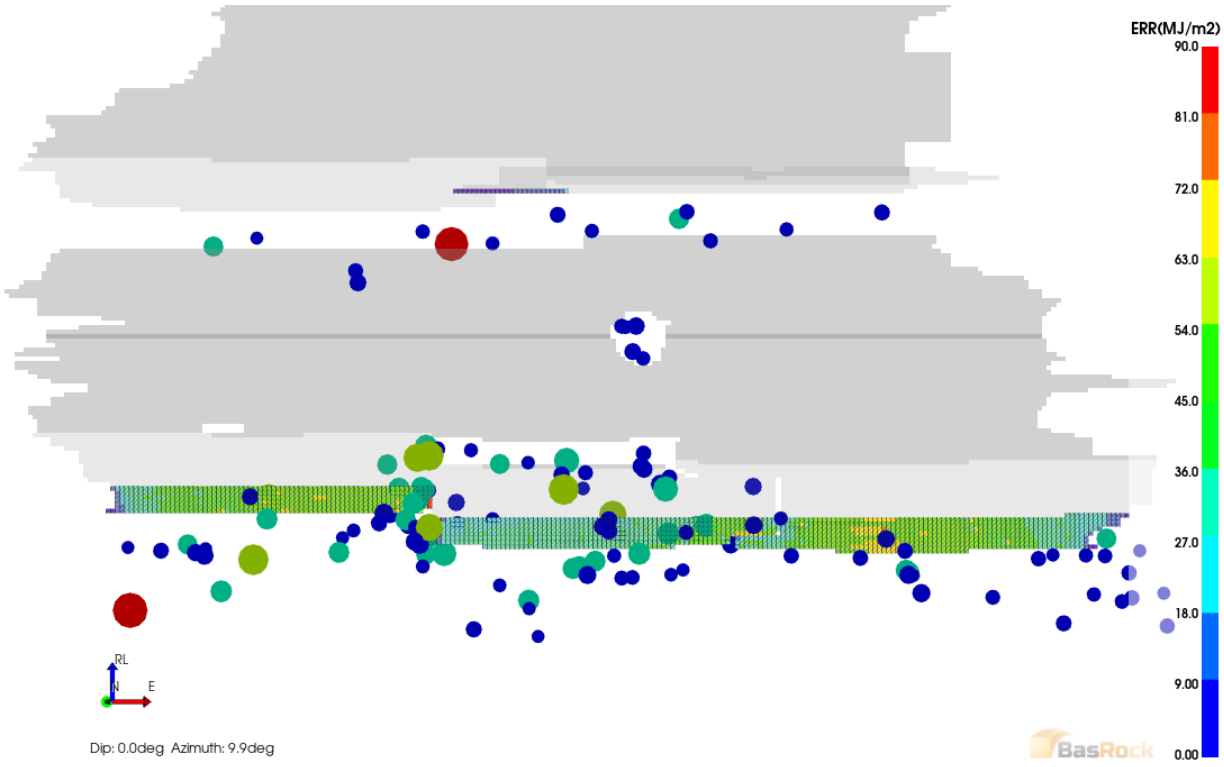

(a)

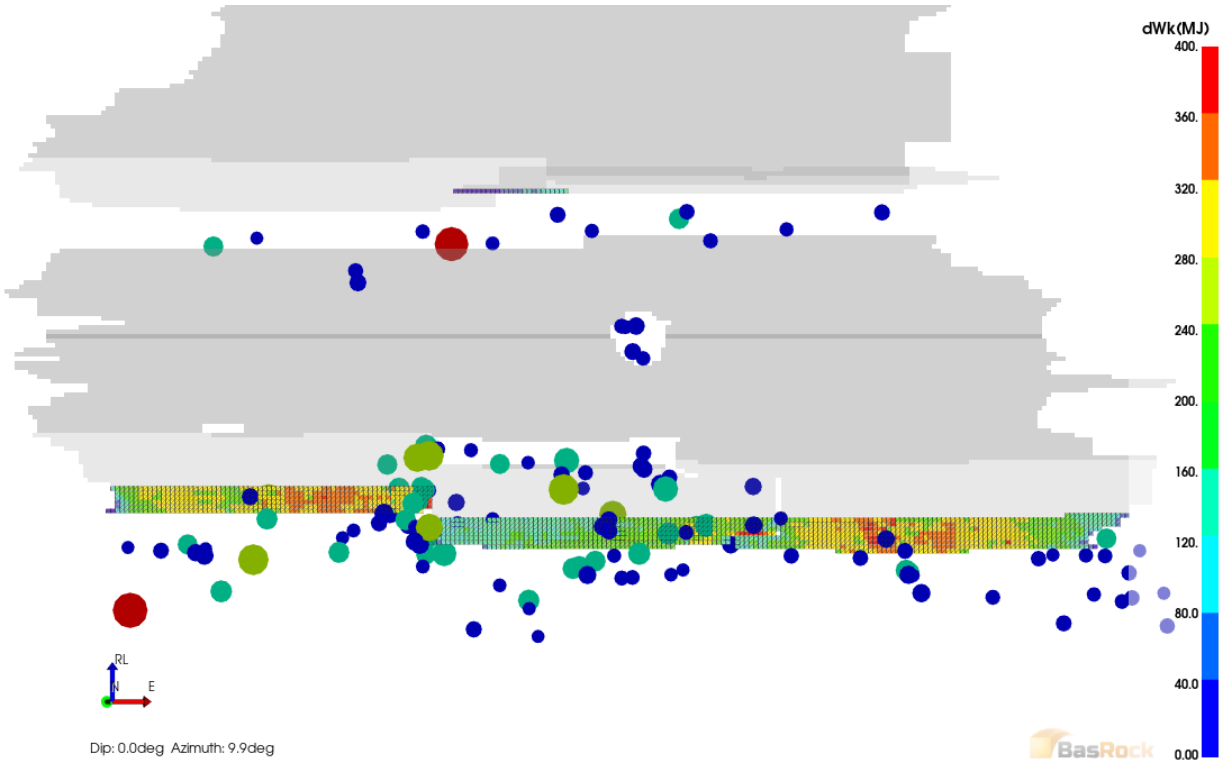

(b)

Figure 4 Computed energy release per DD element for the 2016 extraction with the recorded large seismic events (≥ 1MW) projected onto the 30-Vein, looking north. (a) Computed energy release rate; (b) computed W_k

Each annual production period was compiled in this manner and further combined into their respective mining period. The weighted (by area mined) average annual energies are summarised in Table 1.

Table 1 Energy release per mining period in the Gold Hunter

Mining period	ERR $_{w.avg.}$ (MJ/m^2)	$W_{k\ w.avg.}$ (MJ)	$\eta_{w.avg.}$	η_{max}
1997–2016	27	301,062	0.08%	0.14%
2017–2019	43	64,636	0.02%	0.03%
2020–2021	46	383,846	0.03%	0.04%

As observed, the 2020–2021 mining period released (numerically) the most energy numerically, followed by the 2017–2019 period. This makes sense as the mining front progresses deeper into larger abutting stresses. However, after computing the seismic efficiency (η), defined as the quotient of recorded E_S to numerical W_k, it was observed that these two last periods released less seismic energy than anticipated by the model. Therefore, the largest weighted (by recorded seismic energy) average annual seismic efficiency was observed at 0.08% for the 1997–2016 mining period, with a maximum annual seismic efficiency of 0.14%. These ratios appear low but agree with other findings from the literature, which assume the elastic rock mass assumption (Spottiswoode et al. 2008).

Historically, the BEM elastic assumption is suitable for modelling mine-wide tabular deposits. For a continuous narrow stope, the leading edge creates a (small) local non-linear process zone of damaged material bowing at the advance of the cut. In contrast, the rest of the previously mined stope boundary falls into relaxation. This stress process is similar to an expanding Griffith crack. However, the elastic assumption overestimates the stress at the tip of the mining front where the fracture zone is located (the actual mining face). In reality, the stope heading in the GH shows apparent signs of rock mass yielding response. Therefore, it is recognised

that the elastic assumption used in the BEM model over-predicts the ERR and the kinetic energy release parameters. An option exists to cap the stress at the peak or residual strength of the rock mass, but the rock mass yielding response is insufficiently known at this point to allow for calibration. We wanted to model as simply as possible with minimal assumptions, yet still allowing us to quantitatively compare between production periods.

Nonetheless, this analysis infers a change in rock mass response to mining per period. This observation is further expanded in the following sections.

4.2 Empirical seismic relationship to the ERR

To differentiate these mining periods further, a plot establishing the relationship between seismic events, volume mined, and ERR was assembled per annual period (Figure 5). The best fit GH trend line was computed for the 1997–2016 mining period, presenting an RMSE of +0.578. However, the RMSE of the two subsequent periods is +0.822. Therefore, the chart over-predicts seismic occurrence for the 2017–2021 mining periods. As observed, the number of occurring seismic events larger than +1 MW has significantly reduced during those two mining periods except in 2017, where a higher mining rate impacted the latter in the first quarter of that year, which inevitably released several larger seismic events, better matching the GH trend. However, the subsequent mining years present distinct operational changes where the mining rate (during 2017–2019) was reduced to ~15% of that typically observed for LFUL while staying within 87% of that for UCB (during 2020–2021). The increase in ERR reflects the impact of mining depth observed from 2017–2021 by ~48 m. Overall, these new results show a drop of about one large seismic event (MW > +1) per 1,000 m^3 mined from those previously analysed.

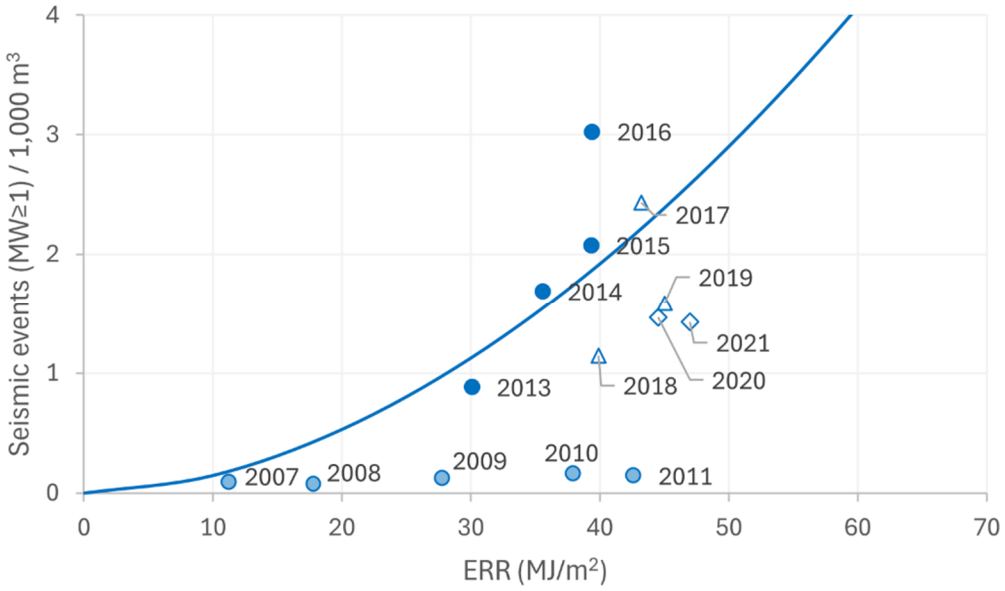

Figure 5 Relation between frequency of seismic occurrence, volume mined, and energy release rate per mining period in the Gold Hunter. The trend line is generated from the 1997–2016 mining period (blue-infilled circular markers). Note that the light-blue markers refer to the MP250 epoch

4.3 Comparison to South African practice

An attempt was made to compare the GH's empirical seismic release plot to those developed by COMRO (1988). These plots are often cited as seismic hazard potential charts for rockbursting and seismic occurrences. They are found in tabular hard rock mine handbooks like that of Jager & Ryder (1999). Figure 6 shows the GH trend line derived for 1997–2016 against the plot for the Ventersdorp Contact Reef (VCR), and the Southern O.F.S and Central Rand Mines. Note that the VCR plot was borrowed from the rockbursting

relationship to energy release, as it is assumed that large events (≥ +1 MW) were needed to cause rockbursts to manifest. Interestingly, the GH's empirical seismic hazard potential plot is bound within the two South African design plots. In addition, ERR set to 30 indicates the onset of one large event per 1,000 m^3 extracted. This ERR threshold is often regarded in South African design for the onset of moderate to severe seismicity (Jager & Ryder 1999).

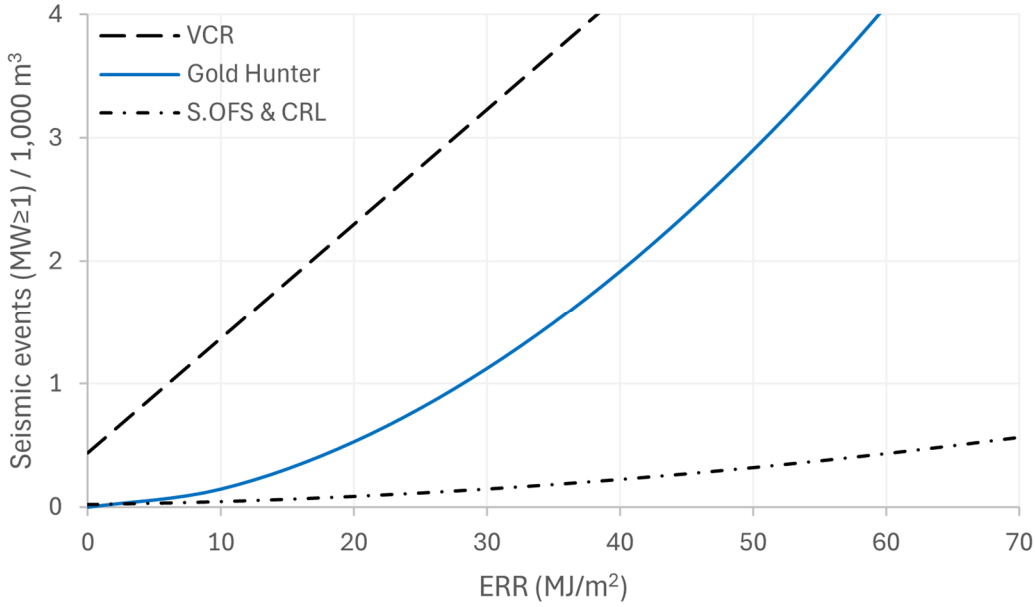

Figure 6 Comparison of empirically derived seismic release curves between the Gold Hunter and South African practice

5 Conclusion

Three mining periods were derived from the GH since mining was initiated in the deposit. Each mining period provides production and seismic records. The first period, between 1997 and 2016, represents the traditional LFUL mining method on the 30-Vein with an average annual production of 720 tpd. The second period, between 2017 and 2019, accounts for a work stoppage, which reduced production by ~85% to an average annual rate of 110 tpd. The third period, between 2020 and 2021, marked the transition and implementation of the UCB mining method on the 30-Vein, which increased production to an average annual rate of 630 tpd.

These mining periods were numerically assessed by BEM for ERR and W_k. It was found that the two later periods (2017–2019 and 2020–2021) produced the highest energy releases, with ERR > 40, when compared to the first period (1997–2016), releasing ERR 27. These two later periods were marked by a significant reduction in production and the implementation of a new mining method across the 30-Vein, respectively. However, upon determining the ratio of the recorded E_S to the simulated W_k, the seismic efficiency revealed that the two later periods underpredict the seismic energy release. Since no geological changes have been observed near the (deeper) mining front, this attribute infers a possible change in the rock mass response to mine-induced seismicity (i.e. mining rate).

After linking seismic records, volumetric changes, and energy release rates, the empirical design chart for the GH was established from the base case period (1997–2016). Interestingly, this base case fits with those published by COMRO for the VCR and Central Rand Mines, tabular deposits.

Acknowledgement

I want to thank Hecla Mining Company for allowing me to publish this analysis. I would also like to extend my gratitude to the Lucky Friday mine, including mine operations/crews as well as the technical staff.

References

Armatys, M 2023, '*Numerical Seismic Assessment of a Deep and Narrow Tabular Mine*', PhD thesis, Ecole Polytechnique Montreal, Montreal.

Basson, FRP 2021, *GEM4D*, version 1.8.4.6, computer software, BasRock, https://basrock.net/gem4d

Budavari, S 1983, *Rock Mechanics in Mining Practice*, MS(5) The South African Institute of Mining and Metallurgy, Johannesburg.

COMRO 1988, *An Industry Guide to Methods of Ameliorating the Hazards of Rockfalls and Rockbursts*, Research Organisation Chamber of Mines South Africa, Johannesburg.

Cook, NGW, Hoek, E, Pretorius, J, Ortlepp, W, & Salamon, M 1966, 'Rock mechanics applied to the study of rockbursts', *Journal of the South African Institute of Mining and Metallurgy*, vol. 66, no. 10, pp. 695–705.

Hecla 2023, *Innovative Underhand Closed Bench (UCB) Mining Increases Safety and Productivity*, video file, https://www.youtube.com/watch?v=jN7szIFt4EI

Hedley, DGF 1992, *Rockburst Handbook for Ontario Hardrock Mines*, Energy, Mines and Resources Canada, Canada Centre for Mineral and Energy Technology, Ottawa.

Hofmann, G 2012, 'Correlating modelled elastic energy release with recorded seismicity in a deep tabular mine', *Proceedings of the Second Southern Hemisphere International Rock Mechanics Symposium (SHIRMS)*, The South African Institute Of Mining And Metallurgy, Johannesburg, pp. 407–423.

Jager, AJ & Ryder JA 1999, *A handbook on rock engineering practice for tabular hard rock mines*, Safety in Mines Research Advisory Committee (SIMRAC), Johannesburg.

Malan, DF 1999, 'Time-dependent behaviour of deep level tabular excavations in hard rock', *Rock Mechanics and Rock Engineering*, vol. 32, no. 2, pp. 123–155.

Raffaldi, MJ, Seymour, JB, Richardson, J, Zahl, EG, & Board, MP 2019, 'Cemented paste backfill geomechanics at a narrow-vein underhand cut-and-fill mine', *Rock Mechanics and Rock Engineering*, vol. 52, pp. 4925–4940.

Salamon, MDG 1983, 'Rockburst hazard and the fight for its alleviation in South African gold mines', *Rockbursts, Prediction and Control* vol. 20, pp. 11–52.

Salamon, MDG 1984, 'Energy considerations in rock mechanics: fundamental results' *Journal of the Southern African Institute of Mining and Metallurgy*, vol. 84, no. 8, pp. 233–246.

Scheepers, L 2022, 'Rockburst in South African deep level gold mining: What do we know?' *Proceedings of RaSiM 10 Rockbursts and Seismicity in Mines*, Society for Mining, Metallurgy & Exploration, Englewood.

Scheepers, L, Hofmann, G, Morkel, I, & Ashanti, AG 2012, 'The study of seismic response to production for a grid mining layout', *Proceedings of the Second Southern Hemisphere International Rock Mechanics Symposium (SHIRMS)*, The South African Institute Of Mining And Metallurgy, Johannesburg, pp. 387–406.

Spottiswoode, SM, Linzer, LM & Majiet, S 2008, 'Energy and Stiffness of Mine Models and Seismicity', in Y Potvin, J Carter, A Dyskin & R Jeffrey (eds), *SHIRMS 2008: Proceedings of the First Southern Hemisphere International Rock Mechanics Symposium*, Australian Centre for Geomechanics, Perth, pp. 693–707, https://doi.org/10.36487/ACG_repo/808_152

Wiles, TD 2022, *Mine Analysis Package in Three Dimensions*, version 68, computer software, Mine Modelling Pty, Ltd.